Pyrrole-tailed imidazolium surface-active monomers: aggregation properties in aqueous solution and polymerization behavior

Stéphanie Boullanger, Emmanuel Contal, Cédric Buron, Lydie Viau

Pyrrole-tailed imidazolium surface-active monomers: aggregation properties in aqueous solution and polymerization behavior

Stéphanie Boullanger,[a] Emmanuel Contal,[a] Cédric Buron [a] and Lydie Viau [a*]

[a] *Institut UTINAM, UMR CNRS 6213, Univ. Bourgogne-Franche-Comté, Equipe Matériaux et Surfaces Fonctionnels, 16 route de Gray, 25030 Besançon Cedex, France.*

* To whom correspondence should be sent: E-mail: lydie.viau@univ-fcomte.fr

Abstract

Pyrrole-functionalized imidazolium surfactants PyC_nMImBr with different alkyl chain lengths (n = 8, 10, 12) were synthesized and their aggregation properties in water were investigated by tensiometry and conductimetry. These studies show that PyC_nMImBr surfactants present lower critical micellar concentration than their non-functionalized analogues due to both an increased hydrophobicity resulting from the extension of the alkyl chain length upon incorporation of pyrrole but also to the formation of attractive π-π interactions among pyrrole moieties. The areas occupied by PyC_nMImBr molecules are always higher than those of C_nMImBr surfactants showing looser molecular arrangement at the air-water interface due to steric hindrance of pyrrole moieties. ^1H nuclear magnetic resonance measurements have been used to shed light on the structure of the aggregates formed. In all cases, pyrrole is located inside the micellar core but for the shortest alkyl chain length it tends to intercalate between the alkyl chains. Micelles obtained with $PyC_{12}MImBr$ were further used as nano-reactor to prepare water-stable polypyrrole nanoparticles. For this, we conduct the chemical polymerization of pyrrole inside the micelles using $FeCl_3$ as oxidizing agent. Polymerization kinetics were followed by UV-spectroscopy. Combined with Infrared (IR) and Dynamic Light Scattering (DLS) measurements, we confirmed the formation of polypyrrole particles of about 4 nm that were water-stable thanks to the presence of cationic imidazolium functions on their surface.

Keywords

Ionic Liquids, Pyrrole, Polymerization, Self-assembly, Surfmer

1. Introduction

Intrinsically conducting polymers (ICPs) have found a lot of applications like in sensors,[1] anticorrosion coatings,[2] energy storage[3] and optical devices.[4] Increasingly, researchers are applying the knowledge gained in these areas toward biomedical applications including biosensing,[5] drug delivery[6] and implantable medical devices.[7] The majority of these studies have focused on the use of Polypyrrole (PPy) which is biocompatible. However, as many others ICPs, PPy suffers from low solubility which renders its processability difficult. Thus, one way to circumvent this solubility problem is to introduce charged side chains as in polyelectrolytes. Poly(ionic liquids) (PILs), a special class of polyelectrolytes, that contain functional groups derived from ionic liquids monomers (imidazolium or pyridinium cations for instance)[8] have been used as steric stabilizers and as phase transfer agents of polypyrrole thus allowing the transfer of PPy micrometers particles from water to a variety of organic solvent.[9, 10] PILs that possess an intrinsically conducting polymers (ICP) backbone like polypyrrole have been synthesized with the objective to combine ionic and electronic conducting properties in the same polymers.[11] These PIL-ICP hybrids have been shown to be able to disperse multi-wall carbon nanotubes in various solvents. Compared to the use of classical ionic liquids (ILs), the use of PIL-ICP allows a higher wrapping of the carbon nanotubes while providing additional electronic conductivities to the CNTs through the polypyrrole backbone.[12]

Water-soluble ICPs show exceptional fluorescence quenching efficiencies in the presence of oppositely charged acceptors and are of particular interest for imaging, diagnosis, and therapy applications.[13, 14] Besides that, in recent years, special attention has been paid to the development of conjugated polymer nanoparticles (CPNs).[15] Indeed, CPNs possess several advantages for biological imaging and sensing applications like their high brightness, large extinction coefficients, superior photostability, low cytotoxicity, facile chemical synthesis and tunable spectral properties. These CPNs are classically obtained *via* two methods: miniemulsion and reprecipitation. Water-dispersive PPy CPNs of less than 100 nm were synthesized without any template or surfactants by Liao and collaborators using 2,4-diaminodiphenylamine as an initiator in aqueous solution[16] and by Gelling *et al.* using ozone as oxidizing agent.[17]

One other interesting alternative to elaborate water soluble CPNs would be to use surface-active monomers *i.e.* surfmers like pyrrole-functionalized surfactants. To our knowledge, this approach has never been reported before. However, the interfacial and micellar behaviors of pyrrole-functionalized ammonium surfactants were studied and these monomers were further electropolymerized to build well-organized interfacial structures.[18, 19] The surfactant behavior of other pyrrole-based compounds including phosphonate-based ones, has also been studied.[20] Concomitantly, imidazolium and pyridinium-based surfactants bearing a terminal pyrrole group have been also used as structure-directing agent to elaborate ordered mesoporous silica structure. Pyrrole units were easily polymerized *via* chemical oxidation and, consequently, highly ordered hexagonal mesoporous silicas with aligned polypyrrole nanowires in channels were achieved. After silica etching, aligned PPy nanowires were obtained.[21] Using the same surfactant, the latter authors reported the synthesis of PPy capsules with tunable thickness by simple modification of sol-gel conditions.[22] CPNs have been obtained by the microemulsion polymerization method using an imidazolium-functionalized pyrrole monomer containing a short butyl alky chain between each groups and used as sensor in DNA detection.[23] Imidazolium-tailed pyrrole surfactants were more recently used as fluidic light sensing materials for preparing flexible optoelectronic sensors[24] and were also electrochemically polymerized to obtain polypyrrole films with wrinkle structure. This latter method constitutes a way to immobilize ionic liquids on solid surface[25] and can be further used for solid-phase microextraction.[26] Other examples of imidazolium-based surfactants containing a polymerizable monomer include the work of Firestone and co-workers on thiophene-tailed imidazolium[27] and of Zheng and collaborators on carbazole-tailed imidazolium surfactants.[28]

This literature survey indicates that pyrrole-tailed imidazolium PyC_nMImBr molecules have been used for the preparation of different materials such as polypyrrole films, porous materials and PILs. Some of these studies have even taken benefit from the surfactant properties of these molecules to prepare well-structured materials. However, surprisingly, their surfactant behavior has not been studied in detail. Only recently, the aggregation behavior and interfacial electrokinetic properties of $PyC_{12}MImBr$ were studied by dielectric spectroscopy showing spontaneously formation of spherical micelles at concentration higher than the Critical Micellar Concentration (CMC = 8.5 mM).[29]

The main objective of this paper is thus to fill this gap and to exemplify another case of the use of surfactant based-ionic liquids for the elaboration of nanoparticles.[30] In the present paper, surface activities and CMCs were determined by surface tension, conductimetry and

NMR and were compared with data obtained for long alkyl chain imidazolium bromide ILs. As these PyC_nMImBr surfactants can be considered as polymerizable surfactant *i.e.* as surfmers, we studied in the second part of this work, the polymerization ability of one of this surfmer surfactant to produce water-dispersible polymer nanospheres. The chemical structures and designations for these PyC_nMImBr surfactants are shown in Figure 1.

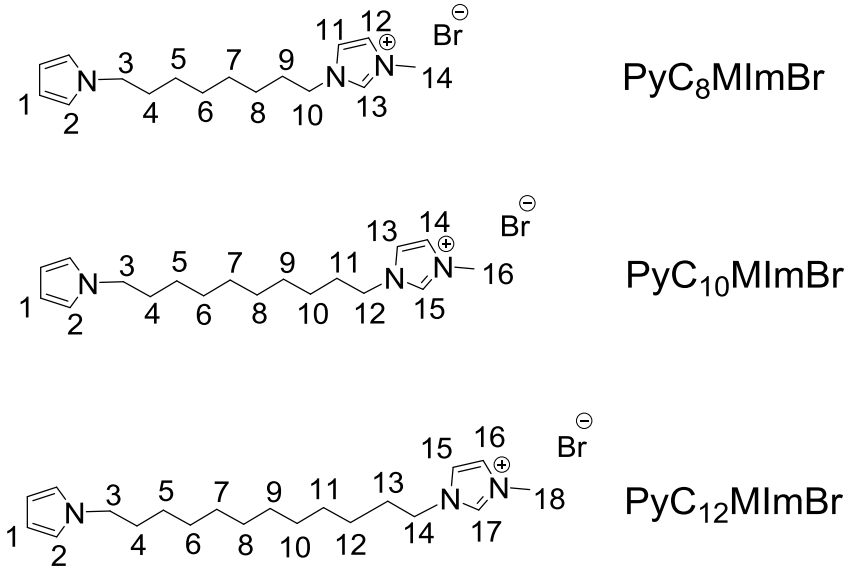

Fig.1. Chemical structures and labeling of the investigated PyC_nMImBr (n = 8, 10 and 12).

2. Experimental

2.1.Materials

The chemicals used were obtained from the following commercial sources: Pyrrole and NaH from Acros Organics® 1,8-dibromooctane, 1,10-dibromodecane and 1,12-dibromododecane from Alfa-Aesar®, *N*-methylimidazole from Aldrich®. Dry DMF was obtained by a solvent purification system PureSolve MD5 from Innovative Technology. Preparative purifications were performed by silica gel flash column chromatography (VWR 40-63 µM). Toluene and solvents used as eluents are off technical grade.

2.2.Synthesis of *N*-Bromoalkyle pyrrole PyC_nBr

General procedure. Dibromoalkane was dissolved at 0°C in 100 mL of dry DMF. In another flask, pyrrole was added to a cooled suspension (0°C) of NaH (60%wt) in dry DMF (100 mL). This mixture was allowed to reach room temperature and stirred for 30 minutes then cooled again to 0°C. The resulting solution was poured into the dibromoalkane solution by

canula. The mixture was allowed to reach room temperature and stirred for 24 hours. The resulting solution was hydrolyzed by addition of water and the product was extracted with AcOEt (3×100 mL). The resulting organic phase was washed with water (3×100 mL), dried over Na_2SO_4, filtered and the solvent was removed under vacuum. The resulting compound was purified by silica gel chromatography (eluent: dichloromethane/petroleum ether, 1:9).

PyC_8Br. General procedure was followed using 1,8-dibromooctane (12.16 g, 44.7 mmol, 1.5 equiv), pyrrole (2 g, 29.8 mmol, 1eq) and NaH (60%wt) (1.31 g, 32.7 mmol, 1.1 equiv). PyC_8Br was obtained as a transparent oil (4.3 g, 56%). ^{1}H NMR (400 MHz, $CDCl_3$): δ = 6.65 (t, J = 2.1Hz, 2H, H_2), 6.14 (t, J = 2.1Hz, 2H, H_1), 3.87 (t, ^3J = 7.1 Hz, 2H, H_3), 3.40 (t, ^3J = 6.8 Hz, 2H, H_{10}), 1.84 (qt, ^3J = 6.8 Hz, 2H, H_9), 1.76 (m, 2H, H_4), 1.45 (m, 2H, H_8), 1.33 (m, 6H, H_5, H_6, H_7). $^{13}C\{^1H\}$ NMR (100.6 MHz, $CDCl_3$): δ =120.5 (C2), 107.9 (C1), 49.7 (C3), 34.0 (C10), 32.8 (C9), 31.6 (C4), 29.1 (C6), 28.7 (C7), 28.1 (C8), 26.7 (C5) ppm. IR (ATR): 3100, 2927, 2854, 1541, 1499, 1459, 1358, 1279, 1256, 1087, 1060, 997, 816, 718, 644, 616, 560 cm^{-1}.

$PyC_{10}Br$. General procedure was followed using 13.41 g (44.7 mmol) of 1,10-dibromodecane, 2 g of pyrrole (29.8 mmol) and NaH (60 wt%) (1.32 g, 32.8 mmol). $PyC_{10}Br$ was obtained as a transparent oil (3.13g, 37%). ^{1}H NMR (400 MHz, $CDCl_3$): δ = 6.66 (t, J = 2.1Hz, 2H, H_2), 6.15 (t, J = 2.1Hz, 2H, H_1), 3.87 (t, ^3J = 7.2 Hz, 2H, H_3), 3.42 (t, ^3J = 7.2 Hz, 2H, H_{12}), 1.85 (qt, ^3J = 7.2 Hz, 2H, H_{11}), 1.77 (m, 2H, H_4), 1.43 (m, 2H, H_{10}), 1.29 (m, 10H, H_5, H_6, H_7, H_8 and H_9). $^{13}C\{^1H\}$ NMR (100.6 MHz, $CDCl_3$): δ =120.5 (C2), 107.8 (C1), 49.7 (C3), 34.1 (C12), 32.9 (C11), 31.6 (C4), 29.5 (C6), 29.4 (C7), 29.3 (C8), 28.8 (C9), 28.2 (C10), 26.8 (C5) ppm. IR (ATR): 3100, 2924, 2853, 1499, 1462, 1357, 1280 1087, 1062, 967, 717, 645, 616, 560 cm^{-1}.

$PyC_{12}Br$. General procedure was followed using 14.67 g (44.7 mmol) of 1,12-dibromododecane, 2 g of pyrrole (29.8 mmol) and NaH (60 wt%) (1.31 g, 32.7 mmol). $PyC_{12}Br$ was obtained as a transparent oil that became solid upon standing in the fridge (4.34 g, 46%).

^{1}H NMR (400 MHz, $CDCl_3$): δ = 6.62 (t, J = 2.1Hz, 2H, H_2), 6.14 (t, J = 2.1Hz, 2H, H_1), 3.86 (t, ^3J = 7.2 Hz, 2H, H_3), 3.41 (t, ^3J = 7.2 Hz, 2H, H_{14}), 1.84 (qt, ^3J = 7.2 Hz, 2H, H_{13}), 1.76 (m, 2H, H_4), 1.42 (m, 2H, H_{12}), 1.30 (m, 14H, H_5, H_6, H_7, H_8, H_9, H_{10}, H_{11}). $^{13}C\{^1H\}$ NMR (100.6 MHz, $CDCl_3$): δ =120.6 (C2), 107.8 (C1), 49.7 (C3), 34.2 (C14), 32.9 (C13), 31.8 (C4), 29.5 (C6, C8, C11 and C12), 29.3 (C7), 28.9 (C9), 28.3 (C10), 26.9 (C5) ppm. IR (ATR): 2923, 2853, 1499, 1461, 1374, 1281 1088, 1063, 967, 717, 647, 616, 560 cm^{-1}.

2.3. Synthesis of Pyrrole-functionalized imidazolium surfactants PyC_nMImBr

General procedure. PyC_nBr was dissolved in 70 mL of toluene before addition of *N*-methylimidazole. The resulting mixture was reflux for 24 hours. After cooling down to room temperature, two phases were formed. The lower phase that contained the product was washed several times with diethyl ether (3×50 mL) and the solvent was evaporated under vacuum.

PyC_8MImBr. General procedure was followed using 7.36 g (28.5 mmol) of PyC_8Br and 2.81 g (34.2 mmol) of *N*-methylimidazole. The final product was recovered as a creamy powder (9.50 g, 98%). m_p = 79°C. ^{1}H NMR (400 MHz, $CDCl_3$): δ = 10.61 (s, 1H, H_{13}), 7.37 (t, ^3J = 1.9 Hz, 1H, H_{12}), 7.28 (t, ^3J = 1.9 Hz, 1H, H_{11}), 6.63 (s, 2H, H_2), 6.11 (s, 2H, H_1), 4.30 (t, ^3J = 7.5 Hz, 2H, H_{10}), 4.11 (s, 3H, H_{14}), 3.85 (t, ^3J = 7.5 Hz, 2H, H_3), 1.89 (m, 2H, H_9), 1.73 (m, 2H, H_4), 1.32 (m, 8H, H_5, H_6, H_7, H_8). $^{13}C\{^1H\}$ NMR (100.6 MHz, $CDCl_3$): δ = 137.6 (C13), 123.6 (C12), 121.9 (C11), 120.5 (C2), 107.8 (C1), 50.1 (C10), 49.5 (C3), 36.7 (C14), 31.5 (C4), 30.2 (C9), 28.8 (C6/C8), 26.5 (C5), 26.1 (C7) ppm. IR (ATR): 3083, 3036, 2926, 2853, 1659, 1564, 1500, 1456, 1377, 1335, 1276, 1152, 1093, 970, 870, 780, 738, 659 cm^{-1}. Anal. Calc for $C_{16}H_{26}BrN_3$ (340.30): %C 56.47, %H 7.70, %N 12.35; found %C 56.33, %H 7.66, %N 12.43.

$PyC_{10}MImBr$. General procedure was followed using 2.96 g (10.3 mmol) of $PyC_{10}Br$ and 0.98 mL (12.4 mmol) of *N*-methylimidazole. $PyC_{10}MImBr$ was obtained as a yellowish oil (2.86 g, 74%). ^{1}H NMR (400 MHz, $CDCl_3$): δ = 10.66 (s, 1H, H_{15}), 7.30 (t, ^3J = 1.9 Hz, 1H, H_{14}), 7.23 (t, ^3J = 1.9 Hz, 1H, H_{13}), 6.64 (t, ^3J = 2.0 Hz, 2H, H_2), 6.12 (t, ^3J = 2.0 Hz, 2H, H_1), 4.30 (t, ^3J = 7.5 Hz, 2H, H_{12}), 4.12 (s, 3H, H_{16}), 3.85 (t, ^3J = 7.5 Hz, 2H, H_3), 1.91 (m, 2H, H_{11}), 1.74 (m, 2H, H_4), 1.28 (m, 12H, H_5, H_6, H_7, H_8, H_9, H_{10}). $^{13}C\{^1H\}$ NMR (100.6 MHz, $CDCl_3$): δ = 137.4 (C15), 123.6 (C14), 121.9 (C13), 120.5 (C2), 107.7 (C1), 50.1 (C12), 49.6 (C3), 36.7 (C16), 31.5 (C4), 30.3 (C11), 29.1 (C6/C7/C8/C9), 26.7 (C5), 26.2 (C10) ppm. IR (ATR): 3136, 3057, 2924, 2852, 1567, 1500, 1460, 1370, 1278, 1167, 1089, 1062, 966, 826, 723, 651, 619 cm^{-1}. Anal. Calc for $C_{18}H_{30}BrN_3.1.5\ H_2O$ (395.73): %C 54.68, %H 8.41, %N 10.62; found %C 54.24, %H 8.14, %N 10.63.

$PyC_{12}MImBr$. General procedure was followed using 7.11 g (22.6 mmol) of $PyC_{12}Br$ and 2.23 g (27.2 mmol) of *N*-methylimidazole. $PyC_{12}MImBr$ was obtained as a yellowish oil (8.19 g, 91%). ^{1}H NMR (400 MHz, $CDCl_3$): δ = 10.76 (s, 1H, H_{17}), 7.24 (t, ^3J = 1.9 Hz, 1H, H_{16}),

7.20 (t, ^{3}J = 1.9 Hz, 1H, H_{15}), 6.64 (t, ^{3}J = 2.0 Hz, 2H, H_2), 6.12 (t, ^{3}J = 2.0 Hz, 2H, H_1), 4.31 (t, ^{3}J = 7.5 Hz, 2H, H_{14}), 4.12 (s, 3H, H_{18}), 3.85 (t, ^{3}J = 7.5 Hz, 2H, H_3), 1.91 (m, 2H, H_{13}), 1.75 (m, 2H, H_4), 1.27 (m, 16H, H_5, H_6, H_7, H_8, H_9, H_{10}, H_{11}, H_{12}). $^{13}C\{^{1}H\}$ NMR (100.6 MHz, $CDCl_3$): δ = 137.7 (C17), 123.5 (C16), 121.8 (C15), 120.5 (C2), 107.8 (C1), 50.3 (C14), 49.7 (C3), 36.9 (C18), 31.5 (C4), 30.3 (C13), 29.3 (C6/C7/C8/C9/C10/C11), 26.8 (C5), 26.3 (C12).ppm. IR (ATR): 3067, 2923, 2853, 1567, 1501, 1456, 1367, 1278, 1167, 1087, 965, 826, 723, 653, 617 cm^{-1}. Anal. Calc for $C_{20}H_{34}BrN_3.1H_2O$ (414.42): %C 57.96, %H 8.75, %N 10.14; found %C 57.92, %H 8.80, %N 10.39.

2.4. Synthesis of Polypyrrole nanoparticles

132 mg (332 mmol) of $PyC_{12}MImBr$ were dissolved in 4 mL pure H_2O (C = 12×CMC), then 2.3 equivalents (220 mg) of $FeCl_3.6H_2O$ was added and the mixture was stirred at room temperature or 50°C.

2.5. Physical measurements and instrumentation

Interfacial tension measurements. Surface tension was measured using a tensiometer Krüss K100 by the Wilhelmy plate method at 25°C. Each measurement was averaged over 20 values. Glass container and plate were cleaned with oxygen peroxide for 10 min and rinsed thoroughly with distilled water. Surface tension was considered at equilibrium when the standard deviation of five consecutive measurements did not exceed 0.10 $mN.m^{-1}$. Samples have been prepared by successive dilutions with Milli-Q water and carefully homogenized.

Conductimetry. The conductivity measurements were performed using a SevenEasy conductivity meter (Mettler Toledo) at 25°C. Before measuring the PyC_nMImBr solutions, the probe was calibrated with a standardized 1413 $\mu S.cm^{-1}$ standard conductivity solution (Mettler Toledo). The measurements were carried out by continuous dilution of a concentrated solution of PyC_nMImBr with Milli-Q water. After any dilution, the solution was stirred and equilibrated for 10 min. Each experiment was repeated in duplicate. Measurements were performed with an uncertainty of less than 0.5%.

Infrared Spectra were recorded with a 4 cm^{-1} resolution on a Bruker vertex70 FTIR spectrometer using a Platinum ATR accessory equipped with a diamond crystal.

NMR. The ^{1}H and ^{13}C NMR spectra were obtained on a Bruker AVANCE 400 HD instrument. ^{1}H chemical shifts were referenced to the proton impurity of the NMR solvent and ^{13}C chemical shifts to the NMR solvent.

UV-visible absorption spectra were measured on a Cary-300 spectrometer with a 300-800 nm scan range, a scan rate of 600 nm.min^{-1} and a resolution of 1 nm.

The hydrodynamic sizes of the particles were measured on a Malvern NanoZS equipped with a He-Ne laser (λ = 632.8 nm) at 25°C using the back-scattered mode at an angle of 173°. The correlation function of Dynamic Light Scattering (DLS) was analyzed with the general-purpose method to obtain the distribution of diffusion coefficients of the solutes. The apparent equivalent hydrodynamic diameters (D_h) were determined from the cumulant method using the Stokes-Einstein equation. Mean diameter values were obtained from triplicate runs.

Elemental analyses were performed on a Flash EA 1112 (Thermofisher) elemental analyzer.

3. Results and discussion

3.1. Surfactants synthesis

Three surfactants PyC_nMImBr containing an imidazolium head and a pyrrole-functionalized long alkyl chains (n = 8, 10 and 12) were obtained by a two steps procedure as described by Zhang and collaborators for PyC_{12}MImBr.[21] The first step consists in the *N*-alkylation of pyrrole by dibromoalkane in the presence of NaH. An excess of dibromoalkane was used to limit the formation of the dipyrrolylalkane. This step is followed by a quaternization reaction using *N*-methyl imidazole (Scheme 1). The structural characterization and the purity of the final products were determined by ^{1}H and ^{13}C NMR, IR spectroscopy and elemental analyses. The ^{1}H NMR spectrum of PyC_8MImBr does not present any unexpected signals from unremoved solvent or unreacted intermediates. Only in the case of PyC_{10}MImBr and PyC_{12}MImBr, small amount of water impurity was found in the ^{1}H NMR spectra at 1.7 ppm. The estimate values of water contents based on NMR integrals match well with those found by elemental analysis. Based on these results the purity of all PyC_nMImBr final compounds was estimated to be superior to 95%. (see experimental section and ESI (Figures S1-S18).

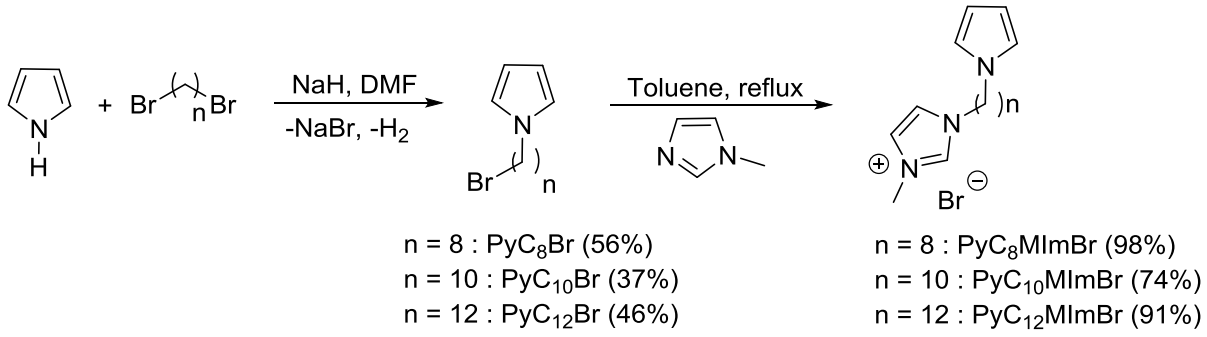

Scheme 1. Synthesis of pyrrole-tailed imidazolium surfactants PyC_nMImBr (n = 8, 10, 12).

3.2. Surface activity

The surfactant behavior of the resulting compounds has been investigated by surface tension measurements. Surface tensions of the solutions *versus* PyC_nMImBr concentration in the logarithmic scale are displayed in Fig. 2. A decrease in surface tension with increasing PyC_nMImBr concentration is observed due to the accumulation of PyC_nMImBr at the air-water surface. In all cases, a minimum of surface tension is observed that is followed by a positive slope and then a plateau. As already described by Goodchild *et al.*, this observation might be ascribed to the formation of surface micelles prior to aggregation leading to a minimum in the area per molecule followed by the recovery of a surface monolayer for concentrations greater than CMC.[31] This phenomena was already observed with other functionalized-imidazolium ionic liquids.[32, 33] It should be noted that the plateau was more easily reached in the following order PyC_8MImBr<$PyC_{10}MImBr$<$PyC_{12}MImBr$ suggesting more favorable aggregation in the same order.

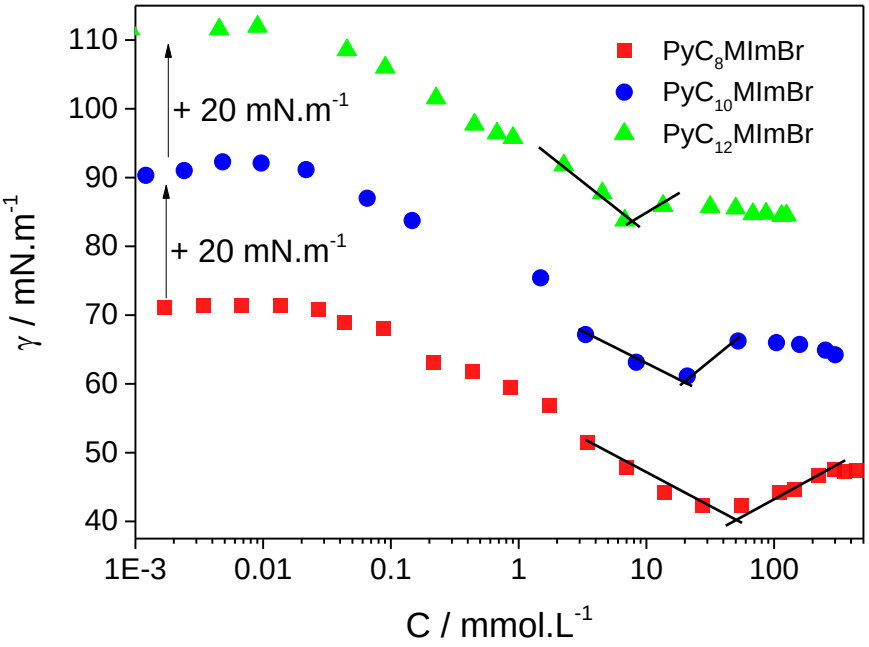

Fig.2. Surface tension isotherms of PyC_nMImBr (n = 8, 10, 12) aqueous solutions at 25°C. For the sake of clarity, the amplitudes for $PyC_{10}MImBr$ and $PyC_{12}MImBr$ have been shifted by +20 $mN.m^{-1}$.

The CMCs were taken at the minimum surface tension which was considered to be the aggregation onset.[34] Table 1 summarizes the CMC values determined from surface tension measurements for PyC_nMImBr. Data previously obtained by other authors by tensiometry for non-functionalized imidazolium surfactants (C_nMImBr) are also included for comparison. As classically observed for conventional cationic imidazolium surfactants, the CMC decreases with an increase of the alkyl chain length.[35] Even though the data reported for C_nMImBr differ from one to the others, it is clear that PyC_nMImBr compounds have slightly lower CMCs than their parent C_nMImBr analogues. Zheng and collaborators reported the self-aggregation of carbazole-tailed imidazolium compounds (CarbazoleC_nMImBr) in aqueous solutions and found even much lower CMCs (CMC = 0.712 mM for CarbazoleC_{10}MImBr *vs* 21 mM for PyC_{10}MImBr and CMC = 0.188 mM for CarbazoleC_{12}MImBr *vs* 8 mM for PyC_{12}MImBr).[28] As in the case of carbazole-tailed imidazolium compounds, the lower CMC values found for our pyrrole-tailed compounds compared to non-functionalized imidazolium ones can be attributed to an increased hydrophobicity resulting from the extension of the alkyl chain length upon incorporation of pyrrole but also to the formation of attractive π-π interactions among pyrrole moieties. As such, our pyrrole-functionalized surfactants present higher CMC values compared to carbazole ones due to weaker π-π interaction among pyrrole moieties and to the lower hydrophobicity of pyrrole compared to carbazole.

The CMC value of PyC_{12}MImBr can also be compared to the one obtained for a dodecyltrimethyl ammonium bromide surfactant containing a pyrrole moiety at the end of the hydrocarbon tail for which a CMC value of 13 mM was determined.[19] In this later case, the CMC is slightly higher than the one of our PyC_{12}MImBr compound due to the presence of a trimethylammonium head group. Indeed, this head group is known to lead to higher CMC values compared to imidazolium ones for which the positive charges are delocalized on the imidazolium ring.[36] The CMC value for PyC_{12}MImBr is also in good agreement with the one reported by Zhao and collaborator (CMC = 8.5 mM) determined by dielectric spectroscopy.[29]

The ability to decrease surface tension was characterized by two other parameters:

- The efficiency of adsorption pC_{20} defined as the negative logarithm of the amphiphilic molecule's concentration required to reduce the surface tension of the pure solvent by 20 $mN.m^{-1}$ (Eq 1)

$$pC_{20} = - \log C_{20} \qquad (1)$$

- The effectiveness of the surface tension reduction π_{CMC} defined as equation (2):

$$\pi_{CMC} = \gamma_0 - \gamma_{CMC} \quad (2)$$

where γ_0 is the surface tension of pure water and γ_{CMC} the surface tension of the solution at the CMC.

pC_{20} values increased with the alkyl chain length, which confirmed a higher efficiency of surfactant activity upon increasing *n*. In our series, a slightly lower value of pC_{20} is obtained for PyC_8MImBr while the values are very close for $PyC_{10}MImBr$ and $PyC_{12}MImBr$. Comparison of the PyC_nMImBr series with the C_nMImBr one shows that the pC_{20} value of $PyC_{10}MImBr$ is higher than its $C_{10}MImBr$ counterpart while pC_{20} values for $PyC_{12}MImBr$ and $C_{12}MImBr$ are nearly identical. Thus, even in the absence of data for C_8MImBr, it can be concluded that PyC_8MImBr and $PyC_{10}MImBr$ have higher adsorption efficiency than C_8MImBr and $C_{10}MImBr$ while $PyC_{12}MImBr$ has only moderate higher efficiency than $C_{12}MImBr$. πCMC varies only slightly with increasing the alkyl chain length.

The area occupied by a surfactant molecule at the air–water interface A_{min} was calculated according to equation (3):

$$A_{min} = \frac{1}{N_A \Gamma_{max}} \quad (3)$$

Where N_A is the Avogadro constant (6.022×10^{23} mol^{-1}), Γ_{max} is the surface excess concentration calculated by applying the Gibbs equation (4) for monocationic surfactant[37]:

$$\Gamma_{max} = -\frac{1}{2RT}\left(\frac{\partial\gamma}{\partial lnC}\right)_T \quad (4)$$

Where R is the gas constant (8.314 J. K^{-1}.mol^{-1}.), T is the absolute temperature and $\frac{\partial\gamma}{\partial lnC}$ is the slope of the surface tension γ *vs* ln C dependence when the concentration is near the CMC.

Recent reports have pointed serious limitations in applying the Gibbs equation accurately to determine surface excess Γ_{max} of cationic surfactants.[38] Indeed, it has been shown that adsorption increases through and above the CMC rendering the polynomial fitting of surface tension unreliable. As such, methods such as neutron reflection that do not require concentrations or activities to determine surface excess would be preferable. Another point that has been pointed out by the same authors is that Wilhelmy plate methods might also lead to uncomplete wetting. The exact values of surface areas reported here should thus be taken

with caution. However, it seems to us that comparison of data obtained by the same method for different compounds gives a correct tendency.

As can be seen in Table 1, the A_{min} value is the highest for PyC_8MImBr (A_{min} = 171 Å^2) and then decreases for $PyC_{10}MImBr$ and $PyC_{12}MImBr$ (A_{min} = 141 and 129 Å^2, respectively) due to closer packing of the monomer at the air/water interface upon increasing the alkyl chain length. This more efficient packing is due to an increase of van der Waals forces between alkyl chains. The areas occupied by PyC_nMImBr molecules are always higher than those of C_nMImBr surfactants showing looser molecular arrangement at the air-water interface due to steric hindrance of pyrrole moieties. The observation of higher surface areas compared to classical imidazolium ionic liquids is also in accordance with the results of Dong and collaborators for carbazole-tailed imidazolium ionic liquids (A_{min} = 191 and 193 Å^2 for n = 10 and 12, respectively). However, as expected from the smaller size of pyrrole compared to carbazole, our surface areas are smaller.[28]

Table 1. Surface properties at 25°C for PyC_nMImBr and C_nMImBr compounds.

Compounds	CMC (mM)	pC_{20}	π_{CMC} (mN.m^{-1})	A_{min} (Å^2)	Γ_{max} (μmol.m^{-2})
PyC_8MImBr	50 ± 5	2.46	29.7	171	0.965
$PyC_{10}MImBr$	20 ± 2	2.65	31.0	141	1.24
$PyC_{12}MImBr$	8 ±1	2.69	31.0	129	1.28
C_8MImBr	170[39], 150[31], 121[40]	-	-	124[39], 60[31]	-
$C_{10}MImBr$	33[39], 40[31], 29.3[41], 20[40]	2.15[41]	33.3[41]	91[39], 48[31], 96.7[41]	1.72[41]
$C_{12}MImBr$	9[39], 10.9[41], 4.3[40]	2.67[41]	33.6[41]	67[39], 86.8[41]	1.91[41]

3.3 Conductivity measurements

Variation of specific conductance of aqueous solutions of PyC_nMImBr as a function of concentration is shown in Figure 3. Two linear regimes in the concentration dependence of the conductivity are clearly observed with a second slope lower than the first one due to the decrease of free charged species in the bulk. The slope break was assigned to the onset of the

CMC. Data obtained by this method are collected in Table 2 and data previously reported for C_nMImBr are also included for comparison. The CMCs values are consistent with the values obtained by surface tension measurements for the longest alkyl chain lengths (n = 10 and 12) but differ in the case of PyC_8MImBr (see table 3). This might be attributed to the presence of the above-mentioned minimum in surface tension measurements. In the case of PyC_8MImBr, this minimum was relatively broad and might have led to some errors in the determination of the CMC. Thus, it is anticipated that conductivity measurements give a more accurate value of the CMC for the shortest chain homologues. In the PyC_nMImBr series, the degree of ionization α determined by Frahm's method *i.e.* as the ratio of the slopes of the linear fragments above and below CMC[42] decreases with the increase of the alkyl chain length from n = 8 to n = 10 and then remains constant with further increase of n. This observation is in line with the observation of constant values of π_{CMC} and pC_{20} for $PyC_{10}MImBr$ and $PyC_{12}MImBr$ (see discussion above).

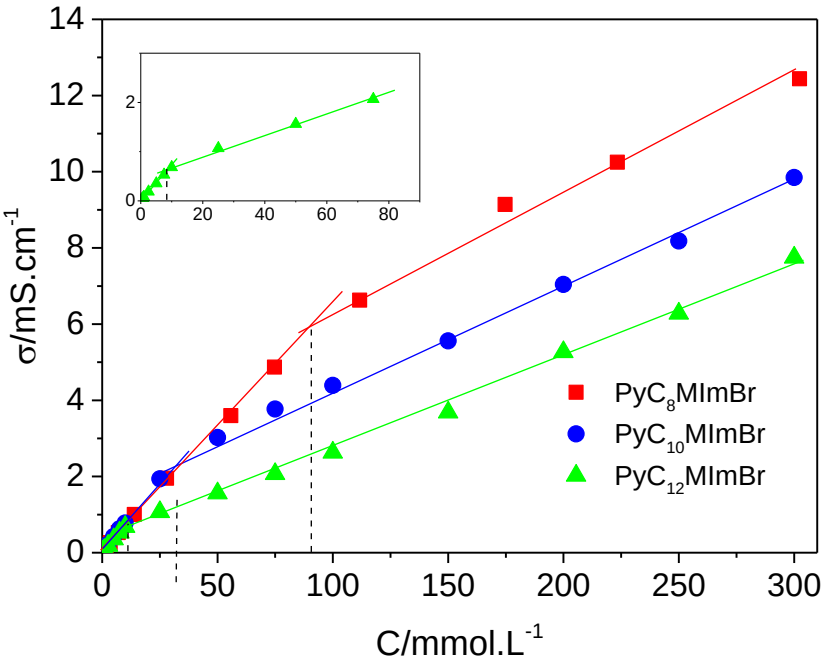

Fig.3. Variation of conductivities *vs* concentrations of PyC_nMImBr (n = 8, 10, 12) aqueous solutions at 25°C.

Table 2. CMCs of PyC_nMImBr determined at 25°C by conductimetry with the corresponding degree of ionization and free energy of aggregation.

Compounds	CMC (mM)	α	ΔG^0_m (kJ.mol^{-1})

PyC_8MImBr	87	0.43	-25.2
$PyC_{10}MImBr$	29	0.34	-30.9
$PyC_{12}MImBr$	7.7	0.34	-36.4
C_8MImBr	160[39], 150[31]	0.57[39]	-20.7[39], -23.5[36]
$C_{10}MImBr$	42[39], 40[31], 41[36], 32.9[41]	0.33[39], 0.29[36], 0.31[41]	-29.7[39], -29.6[36]
$C_{12}MImBr$	10[39], 9.8[36], 8.5[41]	0.26[39], 0.27[36], 0.27[41]	-37.2[39], -37.2[36]

Based on CMCs values determined by conductimetry, we plotted the logarithm variation of CMC (in $mmol.L^{-1}$) against the number of carbons in the alkyl chain length (N_c) (Figure 4 left). This plot follows the Stauff-Klevens rule[43] given by equation (5):

$$\log(CMC) = A - B \times N_c \qquad (5)$$

where A and B are constant for a homologous series of surfactants.

The slope B of this linear variation is -0.26, a value slightly higher than what was reported for C_nMImBr (-0.28)[44] but also higher than the value reported for $CarbazoleC_nMImBr$ compounds (-0.23).[28] As this slope is a measure of the effect of each methylene groups on the CMC it shows that the presence of a pyrrole moiety alters the effect of the methylene group on the CMC compared to non-functionalized C_nMImBr surfactants but this effect is less marked than in the presence of a carbazole unit.

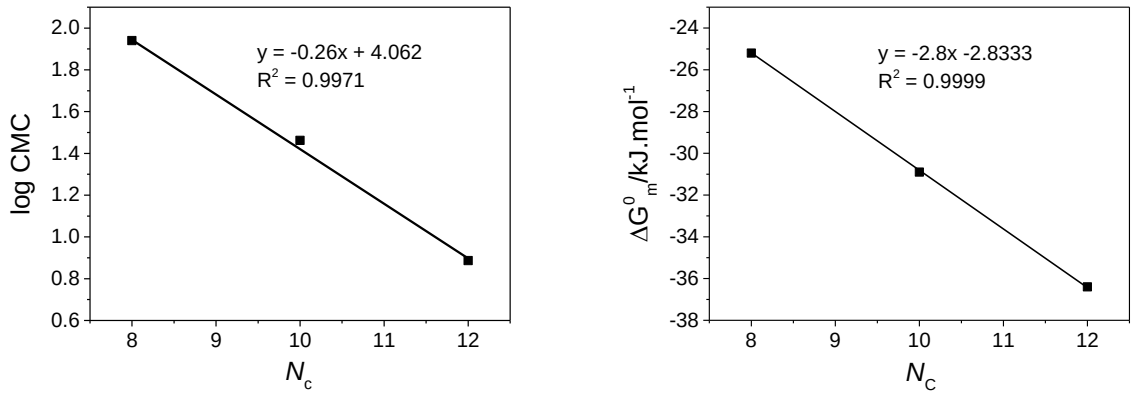

Fig. 4. Logarithm of CMC (mM) (left) and ΔG^0_m (right) as a function of the number of carbon atoms N_c for PyC_nMImBr at 25°C.

The pseudo-phase model of micellization was applied to determine the Gibbs energy of aggregation (ΔG^0_m) according to the following equation:[37]

$$\Delta G_m^0 = (2-\alpha)RT \ln \chi_{CMC} \quad (6)$$

where χ_{CMC} is the critical micellar concentration expressed in mole fraction, α is the degree of ionization.

The obtained ΔG^0_m values are reported in Table 2. Negative values of ΔG^0_m indicate the spontaneity of the micellization process and ΔG^0_m becomes more negative with an increase in the alkyl chain length/hydrophobicity. As previously reported, ΔG^0_m could be divided into contributions from the head group $\Delta G^0_{m,\ head\ group}$, the methylene group of the hydrophobic chain $\Delta G^0_{m,\ CH2}$ and the terminal group of the alkyl chain $\Delta G^0_{m,\ terminal}$ (equation 7).[45] These contributions express the fact that aggregates form under the influence of both attractive and repulsive forces. Attractive forces are associated with the poor solubility of alkyl chains, while effective repulsive forces result from the high solubility of head groups.

$$\Delta G^0_{m} = \Delta G^0_{m,\ head\ group} + \Delta G^0_{m,\ terminal} + N_c\, \Delta G^0_{m,\ CH2} \quad (7)$$

The plot of ΔG^0_m versus nCH_2 (N_c) is presented in Figure 4 (right). It gives a straight line with an intercept equal to $\Delta G^0_{m,\ head\ group} + \Delta G^0_{m,\ terminal}$ and a slope equal to $\Delta G^0_{m,\ CH2}$. Data obtained for PyC_nMImBr were compared to those reported by Wang *et al.* for C_nMImBr.[45] The $\Delta G^0_{m,\ CH2}$ values are close ($\Delta G^0_{m,\ CH2}$ = -2.80 kJ.mol^{-1} for PyC_nMImBr and -2.96 kJ.mol^{-1} for C_nMImBr). However, for PyC_nMImBr the $\Delta G^0_{m,\ head\ group} + \Delta G^0_{m,\ terminal.}$ term is higher than for C_nMImBr (-2.83 kJ.mol^{-1} and -3.77 kJ.mol^{-1}, respectively). As the two series are composed of the same imidazolium head group and the same anion, this difference might be attributed to the presence of a pyrrole group which is less hydrophobic than the methyl group in C_nMImBr.

3.3. ^{1}H NMR spectra

The ^{1}H NMR spectra of the compounds with the shortest alkyl chain length (PyC_8MImBr) and the longest alkyl chain length (PyC_{12}MImBr) were registered in D_2O at different concentrations (Figure S19 and S21). For all concentrations considered in this work, the chemical shifts δ_{obs} for the different protons of PyC_nMImBr are summarized in Supporting Information (Tables S1 and S2). The difference $\Delta\delta$ obtained for different protons between the chemical shifts measured at the highest concentration δ_{max} and those obtained at the lowest concentration δ_{min} are shown in Figure 5. All protons of PyC_8MImBr move upfield ($\Delta\delta < 0$) and the shift is much more important for the protons of the pyrrole ring (H1 and H2) or close to it (H3 and H4) (see Figure 1 for protons attribution). In this latter case also, there is a

pseudo linear variation of the chemical shift for the protons of the alkyl chain between the pyrrole and the imidazolium rings. The alkyl protons close to the pyrrole ring (H3 and H4) undergo the more important upfield shift and this shift decreases as the protons are located further away from the pyrrole ring. For $PyC_{12}MImBr$, the protons of the pyrrole moiety and close to it move also upfield. However, the protons of the CH_2 close to the imidazolium ring (H13 and H14) and those of the imidazolium ring (H15-H17) do not shift significantly.

For surfactants bearing only a classical alkyl chain, a downfield shift off the ^1H NMR chemical signals is commonly observed for the protons of the alkyl chains upon aggregation due to a polarity decrease when going from the aqueous phase to the micellar core.[46] Other studies have demonstrated that, for surfactants with aromatic counteranions for instance, upon incorporation of these aromatic anions into surfactant micelles, two additional effects are observed. Aromatic protons move upfield upon intercalation into the micelles. Additionally, protons of the alkyl chain of the surfactant in the proximity of the shielding cone of the aromatic ring move upfield. As only the protons located in the field of the ring are shifted, it is possible to provide information on the location of the aromatic ring.[47] The upfield shift of the pyrrole protons thus evidences that the pyrrole is located inside the micellar core. On the other hand, the upfield shift of the protons of the alkyl chain shows that the pyrrole intercalates between the alkyl chain resulting in their upfield shift. The determination of the exact location of the pyrrole ring within the alkyl chains is, in our case difficult, as many protons of the alkyl chain are not discernible one from the others. For PyC_8MImBr, all protons of the alkyl chains undergo the shielding effect meaning that they are all located close to pyrrole moieties. For $PyC_{12}MImBr$, protons of the alkyl chains undergo low shielding meaning that they are not in close proximity to the pyrrole ring. At the same time, the $\Delta\delta$ value for H2 of the pyrrole ring is higher for $PyC_{12}MImBr$ than for PyC_8MImBr ($\Delta\delta$ = -032 and -0.26 for $PyC_{12}MImBr$ and PyC_8MImBr respectively) showing that it is more deeply incorporated into the micelles. Based on these results, a schematic illustration of the proposed structures of micelles formed by pyrrole-alkyl-imidazolium surfactants is presented in Figure 6.

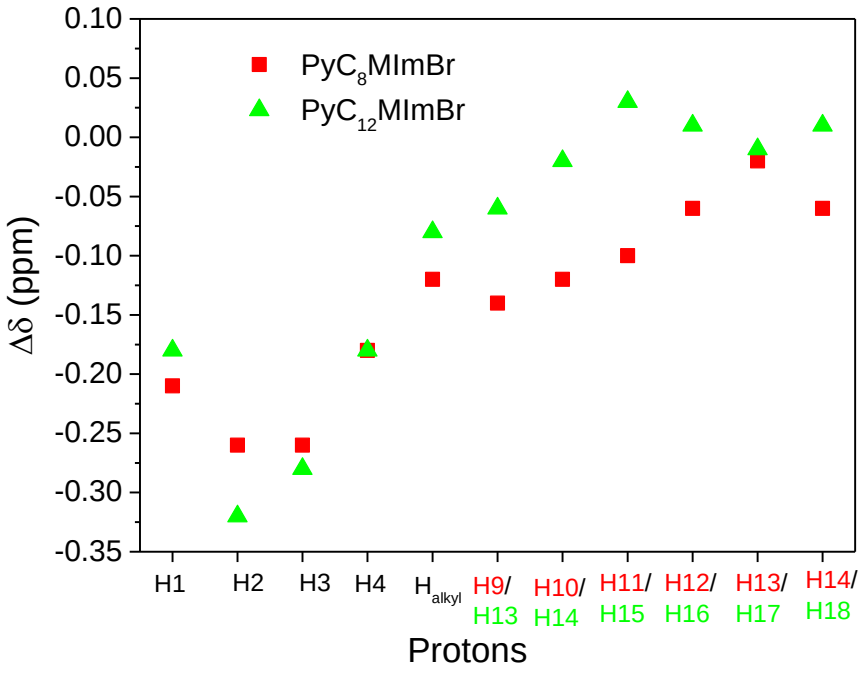

Fig. 5. Amplitude of variation of chemical shifts Δδ for various protons for PyC_8MImBr and $PyC_{12}MImBr$ in D_2O at 25 °C.

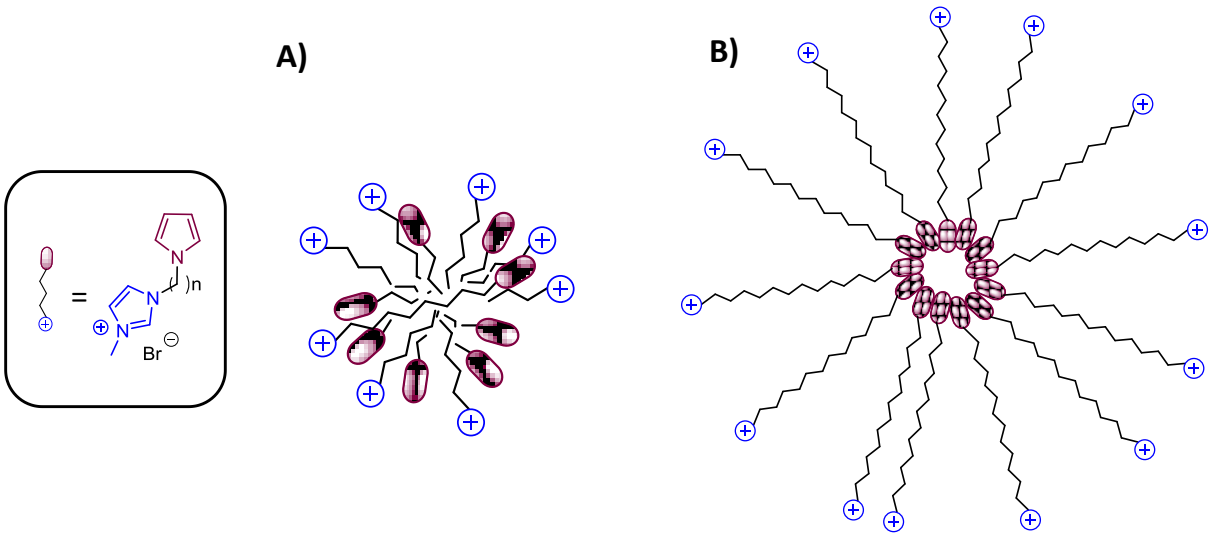

Fig. 6. Schematic representation of the proposed structures of micelles formed with A) PyC_8MImBr and B) $PyC_{12}MImBr$.

It has been shown that ^1H NMR chemical shifts can be used to determine the CMC of surfactants. [48] Under fast exchange occurring on the NMR time scale, the observed

chemical shift for a corresponding proton is a weight average of the monomer (δ_{mono}) and micelle (δ_{mic}) chemical shifts which can be expressed as equation (7):

$$\delta_{obs} = \delta_{mon}\left(\frac{C_{mon}}{C}\right) + \delta_{mic}\left(\frac{C_{mic}}{C}\right) \qquad (7)$$

Where C_{mon}, C_{mic} and C are the concentrations of surfactant monomers, surfactant in micelles and total surfactants in solution, respectively. Above the CMC, it is assumed that the free monomer concentration remains constant so that C_{mic} = C - CMC. Inserting this relation in equation (7) gives equation (8):

$$\delta_{obs} = \delta_{mic} - \left(\frac{CMC}{C}\right)(\delta_{mic} - \delta_{mon}) \qquad (8)$$

According to equation 8, the plots of δ_{obs} versus 1/C should give two straight lines with their intersection corresponding to CMC.

Figure 7 shows the variation of δ_{obs} of the H2 protons of the pyrrole ring versus 1/C for PyC_8MImBr and $PyC_{12}MImBr$ (see figure 1 for protons attribution). As expected, two straight lines are obtained in each case and CMCs values determined from these plots are summarized in table 3. These values are in good agreement with those obtained by conductimetry. Note that same results were obtained considering other protons (Figures S20 and S22).

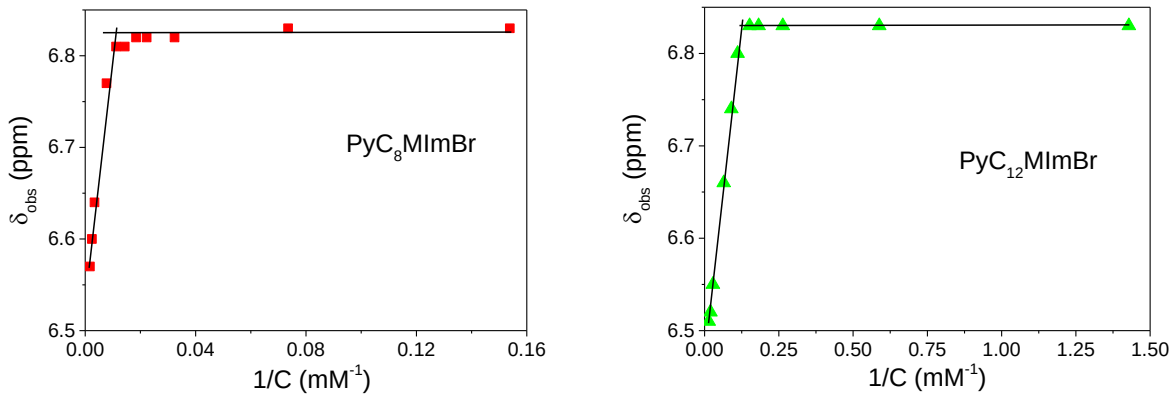

Fig. 7. Chemical shift δ_{obs} as a function of 1/C for H2 for PyC_8MImBr (left) and $PyC_{12}MImBr$ (right) at 25°C

Table 3. CMCs (mM) values of PyC_nMImBr as determined from different methods at 25°C.

Compounds	^{1}H NMR	Surface tension	Conductimetry
PyC_8MImBr	89	50 ± 5	87
$PyC_{10}MImBr$	nd	20 ± 2	29
$PyC_{12}MImBr$	8	8 ±1	7.1

3.4. Polymerization

The chemical polymerization of pyrrole inside micelles was reported by Zhang and collaborators using $FeCl_3$ as oxidizing agent. Micelles were obtained by the self-assembly of different cationic surfactants used as template (cetyltrimethylammonium bromide (CTAB) or dodecyltrimethylammonium bromide (DTAB)). Polypyrrole-sphere like nanostructures with diameters ranging from 35 to 70 nm were obtained. [49]

In order to generate water-stable polypyrrole particles, we tested our ionic surfactants as functional surface-active monomers (surfmers). We focus our study on $PyC_{12}MImBr$ which acts as better surfactant (lower CMC). We thus performed the chemical polymerization of $PyC_{12}MImBr$ in the same conditions as Zhang and collaborators, using a concentration equal to 12 times the CMC and $FeCl_3$ as the oxidant (2.3 eq). Polymerization reactions were performed at room temperature and 50°C and kinetics were followed by UV-visible spectroscopy.

As can be seen on figure 8, the monomer $PyC_{12}MImBr$ does not absorb between 300 and 800 nm (black curve). After addition of $FeCl_3$ (red curve) a strong band at 300 nm is clearly observed due to the absorption of $FeCl_3$.[50] After 4 days, a band at about 480 nm is observed characteristic to the formation of polypyrrole. This spectrum is in accordance with the one obtained for polypyrrole nanospheres reported by Vetter *et al*.[17] The intensity of this band slightly increases with time but the process is quite slow since the absorbance increases slightly during 4 weeks. As can be seen from the picture on figure 9, the sample presents a brown colour characteristic to the formation of polypyrrole.

In order to improve the polymerization kinetics, the same experiments were then realized at 50°C, a temperature at which the micelles were found to be stable (Figure 9). As the same concentrations were used at room temperature and 50°C, the intensity of the absorption bands

can be compared between the two experiments. Clearly, the band at 480 nm is much more intense when the reaction is performed at 50°C meaning that the kinetic of the polymerization was increased upon heating[51] and that the amount of polypyrrole formed was more important. This band extends also up to 550 nm due to partial oxidative doping of the polypyrrole.[50, 52]

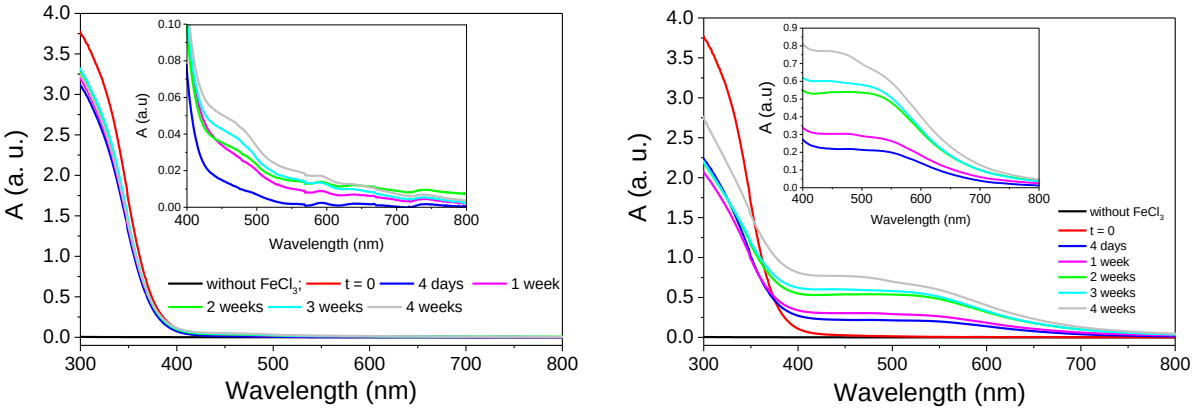

Fig. 8. UV-Visible spectra recorded during polymerization of $PyC_{12}MImBr$ (C= 12× CMC) at room temperature (left) and 50°C (right) with corresponding pictures of the solutions obtained at the end of polymerization.

Figure 9 presents the aggregates size distribution before and after polymerization performed at room temperature. Before polymerization, the $PyC_{12}MImBr$ solution is composed of micelles with a hydrodynamic diameter D_h of 1.4 ± 0.5 nm about twice the length of one surfactant. Note that the same distribution was obtained even after several weeks meaning that micelles were stable for weeks. After 4 weeks of polymerization at room temperature, micelles were still present, but with an average diameter D_h = 4.3 ± 1.5 nm. Micelles swelled because the pyrrole moieties take more space in the core of micelles when they are polymerized. Thus, the surfactants chains were disturbed in their packing and finally the micelles were bigger. The inset in Figure 9 illustrates the water-stability of the resulting polypyrrole nanoparticles.

Even though the kinetic was increased at 50°C, DLS measurements obtained in this case evidenced multimodal distributions (results not shown). Thus, uniformed size particles of polypyrrole could not be obtained under this condition.

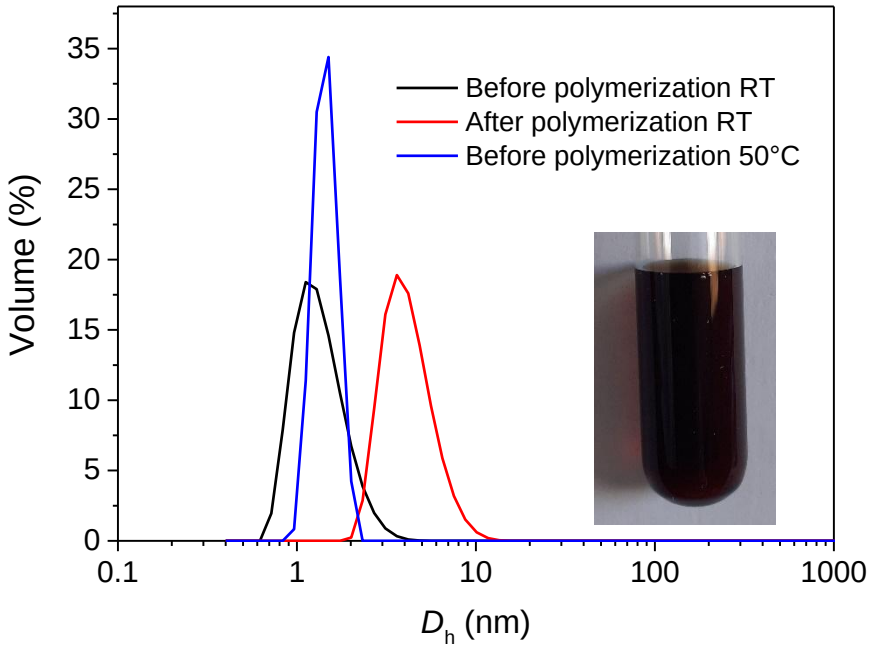

523

524 **Fig. 9.** Size distribution of polypyrrole particles obtained from DLS at 25 °C and 50°C of
525 $PyC_{12}MImBr$ before polymerization (black curve) and after polymerization at room
526 temperature (red). The inset shows photographs illustrating the stability of the polypyrrole
527 particles in water.

528 After polymerization, the sample obtained after 4 weeks at room temperature was lyophilized
529 to register its IR spectrum. Figure 10 disclosed a comparison of the IR spectra of
530 $PyC_{12}MImBr$ before and after polymerization.

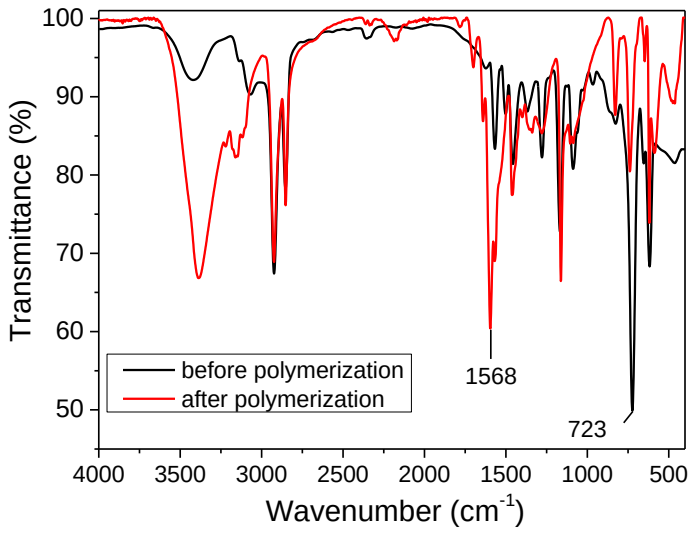

Fig. 10. FT-IR spectra of $PyC_{12}MImBr$ before and after polymerization.

Even though clear attribution of the IR bands is difficult due to an overlapping of the band's characteristics of polypyrrole and those of the imidazolium group, it is clearly observed that after polymerization, the intensity of the peaks at 1568 cm^{-1} increases while, concomitantly, the intensity of the peak at 723 cm^{-1} decreases. The band at 1568 cm^{-1} can be ascribed to the C=C stretching vibration of polypyrrole.[53] As the peak at 723 cm^{-1} is attributed to the α (C-H) bending mode of the pyrrole ring, its significant decrease indicates that α-α coupling of the pyrrole units occurred thus confirming the formation of polypyrrole.[54] Note that similar IR spectra were obtained by Li and collaborators when using $PyC_{12}MImBr$ to prepare ordered silica with polypyrrole in the channels.[21]

4. Conclusion

The surfactant properties of pyrrole-functionalized imidazolium ionic liquids were studied by different techniques. Compared with their non-functionalized analogues, they present lower CMCs and higher adsorption efficiency as expected from the lengthening of the alkyl chain length and the presence of π-π interactions among adjacent pyrrole moieties. However, we also observed a deviation of the evolution of ΔG^0_m values with the number of CH_2 groups in the alkyl chain from what was obtained with classical imidazolium surfactants. Indeed, the contribution of $\Delta G^0_{m,\ terminal}$ in the case of the pyrrole end group is lower than for the methyl group due to its lower hydrophobicity. Additional ^1H NMR experiments have shown that pyrrole is located inside the micellar cores and, in the case of PyC_8MImBr, it intercalates between the alkyl chains.

The chemical polymerization of pyrrole using $PyC_{12}MImBr$ as surfmer was performed both at room temperature and at 50°C. At room temperature, the polymerization is low but results in the formation of polypyrrole nanoparticles with hydrodynamic diameters D_h of about 4 nm. The stabilization of these particles is ensured by electrostatic repulsions between the imidazolium moieties on their surface. Even though the polymerization kinetic of pyrrole inside the micelles can be accelerate at higher temperature, it does not allow the formation of monodisperse polypyrrole particles.

In this study, we thus develop an easy and simple to implement method to prepare water-stable polypyrrole nanoparticles using ionic liquids-based surfactants. These nanoparticles might find applications as interlayers of organic light emitting diodes (OLEDs), antistatic coatings and as inkjet-printed chemical sensors.

Acknowledgements

The authors would like to thank the OSU Theta for its financial support.

References

[1] M. Ates, A review study of (bio)sensor systems based on conducting polymers, Mater. Sci. Eng., C, 33 (2013) 1853-1859.
[2] D. Aradilla, D. Azambuja, F. Estrany, J.I. Iribarren, C.A. Ferreira, C. Alemán, Poly(3,4-ethylenedioxythiophene) on self-assembled alkanethiol monolayers for corrosion protection, Polym. Chem., 2 (2011) 2548-2556.
[3] G.A. Snook, P. Kao, A.S. Best, Conducting-polymer-based supercapacitor devices and electrodes, J. Power Sources, 196 (2011) 1-12.
[4] A.O. Patil, A.J. Heeger, F. Wudl, Optical properties of conducting polymers, Chem. Rev., 88 (1988) 183-200.
[5] W.-K. Oh, O.S. Kwon, J. Jang, Conducting Polymer Nanomaterials for Biomedical Applications: Cellular Interfacing and Biosensing, Polym. Rev., 53 (2013) 407-442.
[6] D. Svirskis, J. Travas-Sejdic, A. Rodgers, S. Garg, Electrochemically controlled drug delivery based on intrinsically conducting polymers, J. Controlled Release, 146 (2010) 6-15.
[7] P.M. George, A.W. Lyckman, D.A. LaVan, A. Hegde, Y. Leung, R. Avasare, C. Testa, P.M. Alexander, R. Langer, M. Sur, Fabrication and biocompatibility of polypyrrole implants suitable for neural prosthetics, Biomaterials, 26 (2005) 3511-3519.
[8] J. Yuan, M. Antonietti, Poly(ionic liquid)s: Polymers expanding classical property profiles, Polymer, 52 (2011) 1469-1482.
[9] R. Marcilla, C. Pozo-Gonzalo, J. Rodríguez, J.A. Alduncin, J.A. Pomposo, D. Mecerreyes, Use of polymeric ionic liquids as stabilizers in the synthesis of polypyrrole organic dispersions, Synth. Met., 156 (2006) 1133-1138.
[10] W. Qian, J. Texter, F. Yan, Frontiers in poly(ionic liquid)s: syntheses and applications, Chem. Soc. Rev., 46 (2017) 1124-1159.
[11] D. Mecerreyes, Polymeric ionic liquids: Broadening the properties and applications of polyelectrolytes, Prog. Polym. Sci., 36 (2011) 1629-1648.
[12] P. Chatterjee, E.M. Nofen, W.W. Xu, C. Hom, H.Q. Jiang, L.L. Dai, Pyrrole-based poly(ionic liquids) as efficient stabilizers for formation of hollow multi-walled carbon nanotubes particles, J. Colloid Interface Sci., 504 (2017) 140-148.
[13] J. Wang, D. Wang, E.K. Miller, D. Moses, G.C. Bazan, A.J. Heeger, Photoluminescence of Water-Soluble Conjugated Polymers: Origin of Enhanced Quenching by Charge Transfer, Macromolecules, 33 (2000) 5153-5158.
[14] C. Zhu, L. Liu, Q. Yang, F. Lv, S. Wang, Water-Soluble Conjugated Polymers for Imaging, Diagnosis, and Therapy, Chem. Rev., 112 (2012) 4687-4735.
[15] J. Pecher, S. Mecking, Nanoparticles of Conjugated Polymers, Chem. Rev., 110 (2010) 6260-6279.
[16] Y.Z. Liao, X.G. Li, R.B. Kaner, Facile Synthesis of Water-Dispersible Conducting Polymer Nanospheres, ACS Nano, 4 (2010) 5193-5202.
[17] C.A. Vetter, A. Suryawanshi, J.R. Lamb, B. Law, V.J. Gelling, Novel Synthesis of Stable Polypyrrole Nanospheres Using Ozone, Langmuir, 27 (2011) 13719-13728.
[18] I. Berlot, P. Labbe, J.C. Moutet, Adsorption and electrochemical oxidation on carbon of micelle-forming cationic surfactants derived from pyrrole, Langmuir, 16 (2000) 5814-5819.

[19] I. Berlot, Y. Chevalier, P. Labbe, J.C. Moutet, Interfacial and micellar behavior of pyrrole-containing cationic surfactants, Langmuir, 17 (2001) 2639-2646.
[20] S. Oberoi, Y. Lu, G. Busch, E. Jaehne, A. Pich, H.J.P. Adler, Novel modified pyrrole monomers, 2: Behaviour in water solutions, Des. Monomers Polym., 11 (2008) 69-82.
[21] W. Zhang, J. Cui, C. Lin, Y. Wu, L. Ma, Y. Wen, G. Li, Pyrrole containing ionic liquid as tecton for construction of ordered mesoporous silica with aligned polypyrrole nanowires in channels, J. Mater. Chem., 19 (2009) 3962-3970.
[22] C. Lin, W. Zhu, H. Yang, Q. An, C.-a. Tao, W. Li, J. Cui, Z. Li, G. Li, Facile Fabrication of Stimuli-Responsive Polymer Capsules with Gated Pores and Tunable Shell Thickness and Composite, Angew. Chem. Int. Ed., 50 (2011) 4947-4951.
[23] J. Zhao, F. Yan, Z. Chen, H. Diao, F. Chu, S. Yu, J. Lu, Microemulsion Polymerization of Cationic Pyrroles Bearing an Imidazolum-Ionic Liquid Moiety, J. Polym. Sci., Part A: Polym. Chem., 47 (2009) 746-753.
[24] Y. He, X.-Q. Xu, S. Lv, H. Liao, Y. Wang, Dark Ionic Liquid for Flexible Optoelectronics, Langmuir, 35 (2019) 1192-1198.
[25] W. Zhang, Y. Li, C. Lin, Q. An, C. Tao, Y. Gao, G. Li, Electrochemical polymerization of imidazolum-ionic liquids bearing a pyrrole moiety, J. Polym. Sci., Part A: Polym. Chem., 46 (2008) 4151-4161.
[26] A.M. Devasurendra, C. Zhang, J.A. Young, L.M.V. Tillekeratne, J.L. Anderson, J.R. Kirchhoff, Electropolymerized Pyrrole-Based Conductive Polymeric Ionic Liquids and Their Application for Solid-Phase Microextraction, ACS Appl. Mater. Interfaces, 9 (2017) 24955-24963.
[27] C.T. Burns, S. Lee, S. Seifert, M.A. Firestone, Thiophene-based ionic liquids: synthesis, physical properties, self-assembly, and oxidative polymerization, Polym. Adv. Technol., 19 (2008) 1369-1382.
[28] B. Dong, Y.a. Gao, Y. Su, L. Zheng, J. Xu, T. Inoue, Self-Aggregation Behavior of Fluorescent Carbazole-Tailed Imidazolium Ionic Liquids in Aqueous Solutions, J. Phys. Chem. B, 114 (2010) 340-348.
[29] X. Fan, K. Zhao, Aggregation behavior and electrical properties of amphiphilic pyrrole-tailed ionic liquids in water, from the viewpoint of dielectric relaxation spectroscopy, Soft Matter, 10 (2014) 3259-3270.
[30] O.A. El Seoud, N. Keppeler, N.I. Malek, P.D. Galgano, Ionic Liquid-Based Surfactants: Recent Advances in Their Syntheses, Solution Properties, and Applications, Polymers, 13 (2021) 1100.
[31] I. Goodchild, L. Collier, S.L. Millar, I. Prokeš, J.C.D. Lord, C.P. Butts, J. Bowers, J.R.P. Webster, R.K. Heenan, Structural studies of the phase, aggregation and surface behaviour of 1-alkyl-3-methylimidazolium halide + water mixtures, J. Colloid Interface Sci., 307 (2007) 455-468.
[32] M.T. Garcia, I. Ribosa, L. Perez, A. Manresa, F. Comelles, Aggregation Behavior and Antimicrobial Activity of Ester-Functionalized Imidazolium- and Pyridinium-Based Ionic Liquids in Aqueous Solution, Langmuir, 29 (2013) 2536-2545.
[33] M.T. Garcia, I. Ribosa, L. Perez, A. Manresa, F. Comelles, Self-assembly and antimicrobial activity of long-chain amide-functionalized ionic liquids in aqueous solution, Colloids Surf., B, 123 (2014) 318-325.
[34] A. Modaressi, H. Sifaoui, M. Mielcarz, U. Domańska, M. Rogalski, Influence of the molecular structure on the aggregation of imidazolium ionic liquids in aqueous solutions, Colloids Surf., A, 302 (2007) 181-185.
[35] J. Łuczak, J. Hupka, J. Thöming, C. Jungnickel, Self-organization of imidazolium ionic liquids in aqueous solution, Colloids Surf., A, 329 (2008) 125-133.

[36] W.L. Zhang, Y.X. Wang, X.Y. Lan, Y. Huo, Imidazolium-based ionic liquids as electrolyte additives for high-voltage Li-ion batteries, Res. Chem. Intermed., 46 (2020) 3007-3023.
[37] M. J. Rosen, Surfactant and Interfacial Phenomena, Wiley-Intersciences, John Wiley & Sons, New Jersey, 2004, 2004.
[38] P.X. Li, R.K. Thomas, J. Penfold, Limitations in the Use of Surface Tension and the Gibbs Equation To Determine Surface Excesses of Cationic Surfactants, Langmuir, 30 (2014) 6739-6747.
[39] A. Cornellas, L. Perez, F. Comelles, I. Ribosa, A. Manresa, M.T. Garcia, Self-aggregation and antimicrobial activity of imidazolium and pyridinium based ionic liquids in aqueous solution, J. Colloid Interface Sci., 355 (2011) 164-171.
[40] Q.Q. Baltazar, J. Chandawalla, K. Sawyer, J.L. Anderson, Interfacial and micellar properties of imidazolium-based monocationic and dicationic ionic liquids, Colloids Surf., A, 302 (2007) 150-156.
[41] B. Dong, N. Li, L. Zheng, L. Yu, T. Inoue, Surface Adsorption and Micelle Formation of Surface Active Ionic Liquids in Aqueous Solution, Langmuir, 23 (2007) 4178-4182.
[42] J. Frahm, S. Diekmann, A. Haase, Electrostatic Properties of Ionic Micelles in Aqueous Solutions, Ber. Bunsen-Ges. Phys. Chem, 84 (1980) 566-571.
[43] J. Stauff, Equilibria between molecular dissipated and colloidal substances in aqueous soap dissipation. 1. Chapter: Hydrolysis of fatty acid salts, Z. Phys. Chem. A, 183 (1938) 55.
[44] T. Inoue, H. Ebina, B. Dong, L. Zheng, Electrical conductivity study on micelle formation of long-chain imidazolium ionic liquids in aqueous solution, J. Colloid Interface Sci., 314 (2007) 236-241.
[45] J. Wang, H. Wang, S. Zhang, H. Zhang, Y. Zhao, Conductivities, Volumes, Fluorescence, and Aggregation Behavior of Ionic Liquids [C4mim][BF4] and [Cnmim]Br (n = 4, 6, 8, 10, 12) in Aqueous Solutions, J. Phys. Chem. B, 111 (2007) 6181-6188.
[46] T. Singh, A. Kumar, Aggregation Behavior of Ionic Liquids in Aqueous Solutions: Effect of Alkyl Chain Length, Cations, and Anions, The Journal of Physical Chemistry B, 111 (2007) 7843-7851.
[47] W. Ge, H. Shi, Y. Talmon, D.J. Hart, J.L. Zakin, Synergistic Effects of Mixed Aromatic Counterions on Nanostructures and Drag Reducing Effectiveness of Aqueous Cationic Surfactant Solutions, The Journal of Physical Chemistry B, 115 (2011) 5939-5946.
[48] C. Chachaty, Applications of NMR methods to the physical chemistry of micellar solutions, Prog. Nucl. Magn. Reson. Spectrosc., 19 (1987) 183-222.
[49] X. Zhang, J. Zhang, W. Song, Z. Liu, Controllable Synthesis of Conducting Polypyrrole Nanostructures, The Journal of Physical Chemistry B, 110 (2006) 1158-1165.
[50] B.L. Langsdorf, B.J. MacLean, J.E. Halfyard, J.A. Hughes, P.G. Pickup, Partitioning and Polymerization of Pyrrole into Perfluorosulfonic Acid (Nafion) Membranes, The Journal of Physical Chemistry B, 107 (2003) 2480-2484.
[51] C.C. Bof Bufon, J. Vollmer, T. Heinzel, P. Espindola, H. John, J. Heinze, Relationship between Chain Length, Disorder, and Resistivity in Polypyrrole Films, The Journal of Physical Chemistry B, 109 (2005) 19191-19199.
[52] G. Zotti, S. Martina, G. Wegner, A.-D. Schlüter, Well-defined pyrrole oligomers: Electrochemical and UV/vis studies, Advanced Materials, 4 (1992) 798-801.
[53] M. Omastová, M. Trchová, J. Kovářová, J. Stejskal, Synthesis and structural study of polypyrroles prepared in the presence of surfactants, Synth. Met., 138 (2003) 447-455.
[54] Y. Chen, C.T. Imrie, K.S. Ryder, Pyrrole- and polypyrrole-based liquid crystals, J. Mater. Chem., 11 (2001) 990-995.